Ion velocity evolution with channel width, magnetic topology and propellant in a 200 W Hall thruster

IEPC-2011-123

Presented at the 32nd International Electric Propulsion Conference,
Wiesbaden, Germany
September 11–15, 2011

G. Bourgeois* , A. Lejeune† and S. Mazouffre‡
ICARE - CNRS, Orléans, France

Abstract: Influence of the geometry and magnetic field strength of the thruster on the ion velocity and acceleration pattern is a crucial point for ion engine as it determines to a large extent the performance level. Ion velocity on-axis profiles were studied in a low power permanent magnet Hall thruster for three channel widths, three magnetic magnitudes and two anode mass flow. Ion velocity distribution functions were measured by means of laser induced fluorescence spectroscopy in the near infrared along the channel centerline in the plume near-field. Close examination of ion velocity distribution function reveals new features which could involve charge exchange collisions with the background gas and beams interaction between each side of the channel of the thruster. Xe^+ ion axial velocity is not influenced by the anode mass flow, but strongly affected by the channel width and the magnetic field strength. Maximum velocity is highest for the largest channel and the strongest magnetic field. Change in near-wall conductivity and electron transport in volume through the magnetic barrier are likely to explain this evolution. Study of Kr^+ ion axial velocity revealed features similar to the examination of Xe^+ ion velocity.

Nomenclature

Φ_a	= Anode mass flow rate
B	= Magnetic field
d	= Thruster mean diameter
h	= Channel width
M	= Mirror
P	= Prism
SRM	= Semi Reflective Mirror
U_d	= Discharge Voltage
x	= Position on the axis on the thruster

I. Introduction

Low power Hall thrusters are dedicated to the drag compensation of satellites that orbit in the atmosphere at low altitude, and the orbit control of satellites constellation. Hall thrusters rely on a potential drop and a radial magnetic field, generated either by coils or permanent magnets, to induce a large azimuthal Hall current which in turn generates a thrust in the axial direction through the Laplace force[1] . We aimed at studying the influence of the channel geometry, magnetic field magnitude and propellant on the velocity

*PhD. Student, Electric Propulsion Team, guillaume.bourgeois@cnrs-orleans.fr
†PostDoctoral Research Fellow, Electric Propulsion Team, aurelien.lejeune@cnrs-orleans.fr
‡Research Scientist, Electric Propulsion Team Leader, stephane.mazouffre@cnrs-orleans.fr

of ions and atoms downstream the channel exit plane of the thruster. Velocities were measured by Laser Induced Fluorescence (LIF) spectroscopy in the near infrared. Influence of the channel width and magnetic field magnitude on acceleration pattern of ions was studied with three sizes of ceramic rings and three different magnetic topologies. Xenon and krypton were used as main propellants. In this paper, we first give details on the thruster specifications such as the LIF bench. In Section II, xenon atoms velocity profile in the near-field plume is examined. Then Xe^+ ions are extensively studied with a large 2D map that shows the acceleration pattern. Systematic influence of the channel width, magnetic field magnitude and propellant on the ion velocity is detailed in the following subsections. Measurements of Kr^+ ion velocity are presented in Section V. Conclusions are drawn in the last section.

II. Experimental set up

A. Thruster operating conditions

In this study, we used a 200 W Hall thruster with permanent magnets, called "'Petit Propulseur Innovant"' or PPI, which stands for small innovative thruster[3,4] . The PPI thruster was operated in the NExET facility. Specific Al_2O_3 ceramic rings were made for the PPI so that three different channel widths are available while the channel mean diameter remains constant. The three sections will be referred to as S_0, $2S_0$ and $3S_0$. The S_0 corresponds to the standard section of modern thrusters, determined by the output power and scaling laws based on a large database of Hall Thrusters.[2] The two other channel widths are twice (resp. three times) the standard width. Permanent Samarium Cobalt magnets are used to generate a magnetic field B_0 similar to the standard magnetic topology of modern thrusters. The magnitude of the magnetic field can be changed by adding or removing magnets in the two sides of the channel of the thruster. Two other values of magnetic field were examined, a weaker one B_{low} and a stronger one B_{high}. Strength in the channel exit plane is $B_{low} = 0.6\times B_0$ and $B_{high} = 1.6 \times B_0$.

Operating conditions of the PPI thruster in its original configuration (S_0, B_0) are : a discharge voltage of 200 V, a xenon mass flow $\phi_a = 1$ mg/s and a discharge current of 1 A, with a cathode potential of - (20 $\pm$ 2) V.

B. LIF bench and collection system

The LIF bench used in this study to probe xenon atoms and singly-charged xenon ions and singly-charged ions has been extensively detailed previously[8,9] and references herein.

The set-up is presented in Fig.1. A high power tunable single mode laser diode excites atoms and ions in the near infrared. A high precision wavemeter monitors the laser wavelength. A 2 GHz confocal Fabry Perot interferometer checks constantly the laser mode in order to prevent mode hops during wavelength tuning. A small fraction of the laser beam is taken aside and sent to a photodiode to get information on any change in the laser beam power. Main laser beam is modulated by a mechanical chopper at a frequency close to 2 kHz to allow lock-in detection on the signal. This technique permits to largely increase the signal-to-noise ratio. The laser beam is carried to the back of the NExET vacuum chamber by several optics and reaches the thruster through a BK7 window placed at the back of the tank. It aims at the channel mean diameter in the axial direction as depicted in Fig.2.

The thruster is mounted onto a translation stage placed in the axial direction to enable measurements from the channel exit plane up to 100 mm downstream. A 4 cm focal length lens is used to collect the light emitted by the plasma with a 1:1 optic imaging, at 90 degrees with respect to the beam direction. Light is then carried out of the chamber by a 200 μm optic fiber. Light is filtered by 1 nm bandwidth monochromator. Fluorescence light is converted in electric signal by a low noise photomultiplier tube and analyzed by a lock-in detector.

III. Neutral velocity

Neutral xenon 6s $[1/2]^o_2$ metastable state is probed at 823.1633 nm. Fluorescence is collected at the same wavelength. Xenon atoms velocity was examined from the channel exit plane up to 75 mm downstream, in order to clarify the hypothesis of charge-exchange collisions downstream the ionization zone. Neutral fluorescence profiles, see Fig.3 shows that two populations exist : neutrals with a very low velocity that may come from the background gas, and neutrals with a higher velocity. Both groups merge downstream.

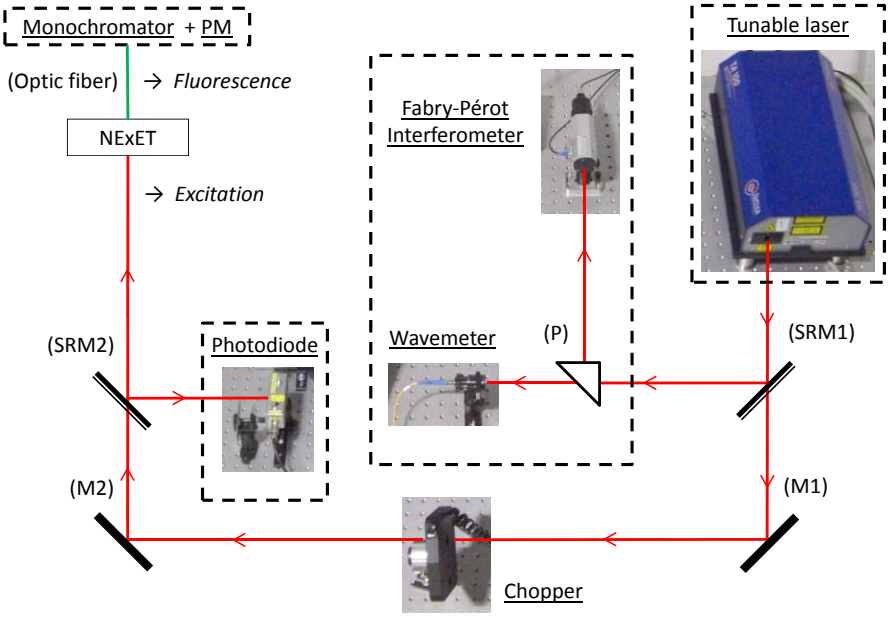

Figure 1. Schematic view of the LIF spectroscopy bench. *M.* stands for Mirror. *SRM.* stands for SemiReflective Mirror. *P.* stands for Prism.

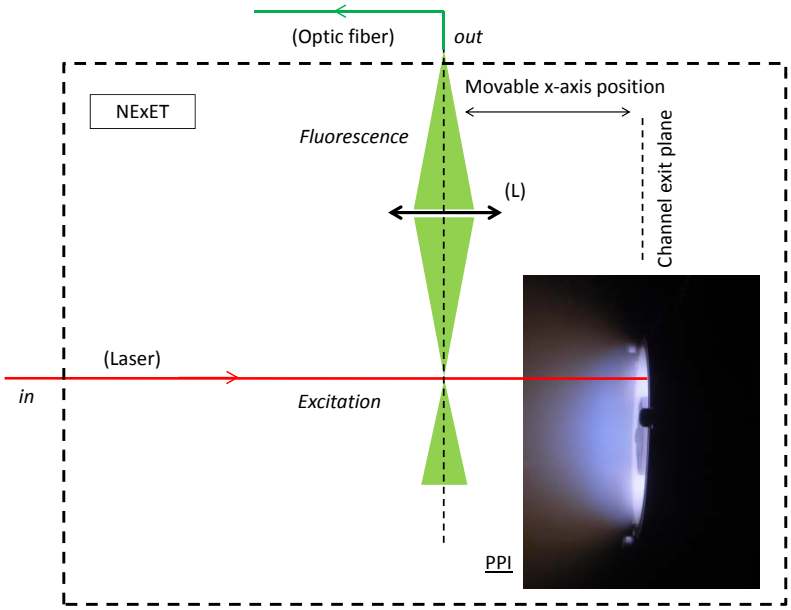

Figure 2. Schematic view of the LIF signal collection optics.

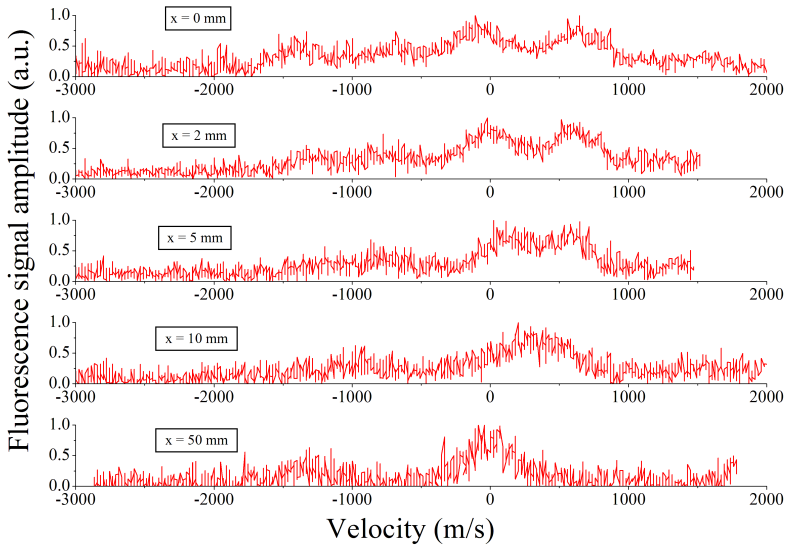

Figure 3. Fluorescence profiles of xenon atoms displayed at several locations along the thruster axis.

Most probable velocity of the two main peaks was solely considered. Note that LIF profiles were smoothed using moving-average method prior to velocity assessment. The two branches pattern is displayed in Fig.4.

Similar features were observed with a 1.5 kW thruster in a previous study[6]. The shape of the velocity profile was explained using analytical treatment and complete modeling of the lineshape as well as numerical simulations performed with a fluid and kinetic hybrid method. Acceleration inside the channel was found to result from three processes, the enhanced ionization of slow atoms which stay longer in the channel, flow expansion, and creation of fast neutrals due to ion recombination on the walls. This phenomenon is likely to explain the velocity of the fastest group of atoms that we observe in the present study in the channel exit plane.

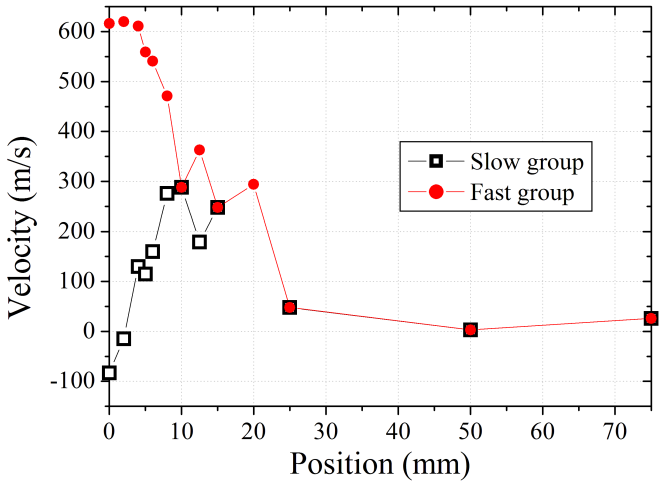

Figure 4. Xenon atoms velocity evolution with position from the channel exit plane. Thruster running parameters are U_d = 200 V and ϕ_a = 1 mg/s and configuration is ($2S_0$, B_0)

Acceleration in the previous study was measured both inside and outside the channel of the thruster. In the present study, measurements were performed only outside the channel. Atoms with a null velocity were not found in the previous study in the channel exit plane. The difference may come from an enhanced interaction with the background gas or the cathode gas flow and a larger invasion of the plasma in the present study.

Deceleration of atoms was found to be due to the residual background gas that invades the neutral beam and collisions between fast and slow atoms that diminish the average velocity. Charge exchange collisions were found to be non negligible in the previous study. Conditions of pressure were similar in both previous and present studies. Charge-exchange collisions thus could explain the slow ions peaks that are observed in the 2D map of Xe^+ VDFs presented in the following section.

IV. Study of Xe^+ ion velocity

A. Spectroscopy and 2D map evolution of the ion VDF.

Xe^+ ions 5d $^2F_{7/2}$ metastable state was probed at 834.7233 nm (air) and fluorescence light was collected at 542 nm. Fluorescence profiles are usually different from the velocity distribution function (VDF) of the examined species because of a large variety of broadening due to the presence of isotopes, hyperfine structure, Zeeman effect due to the magnetic field, and Doppler effect due to species temperature. Operating the deconvolution over all these sources is cumbersome so that only the most probable velocity was retained for the analysis of the acceleration pattern. However, in the case of the transition we selected to study Xe^+ ions, the broadening of the VDF due to the overlap of ionization and acceleration zone is so large compared to all other broadenings that it is reasonable to assume that the fluorescence profile images correctly the VDF[5,8,9] .

Signal-to-noise ratio was good enough so profiles were not smoothed. Uncertainty on the measurement of the most probable velocity is around 150 m/s, due to wavelength measurement and determination of the profiles maximum.

A large map of the evolution with the position of the normalized ions VDFs is drawn in Fig.5 for xenon. Several raw VDFs are also shown aside in Fig.6 in order to help the understanding of the VDFs evolution along the axis of the thruster channel. Discharge voltage was 200 V and discharge current was 1 A with ϕ_a = 1 mg/s. The largest width ($3S_0$) was used at it provided the most stable operation. Magnetic field

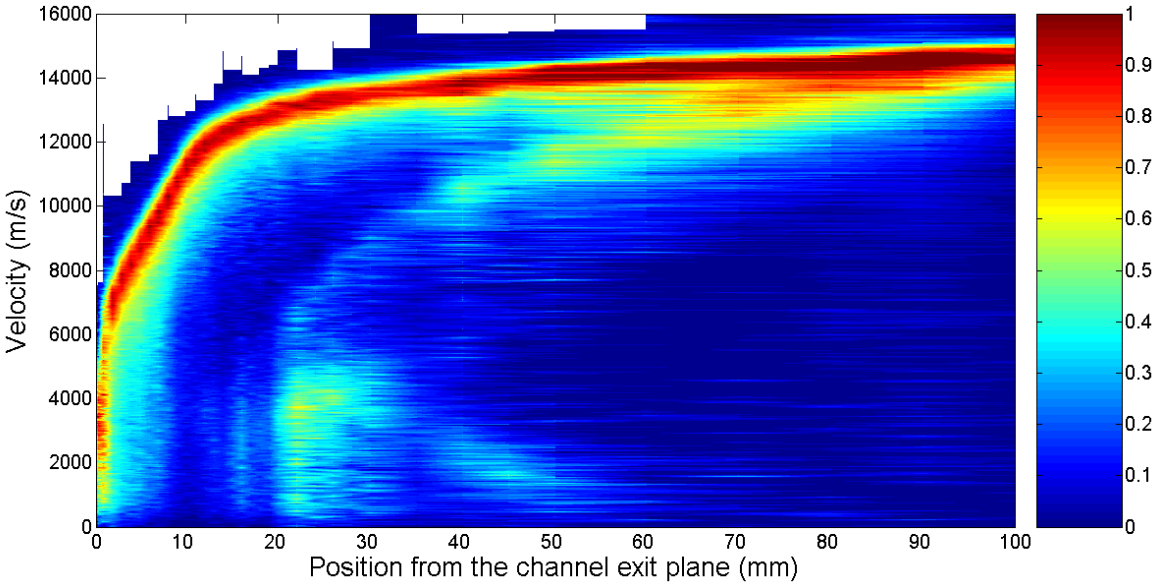

Figure 5. 2D map of the evolution of the Xe^+ ion VDF with the position. Amplitude is given by the colorbar. Thruster running parameters are U_d = 200 V and ϕ_a = 1 mg/s, and configuration is ($3S_0$, B_0)

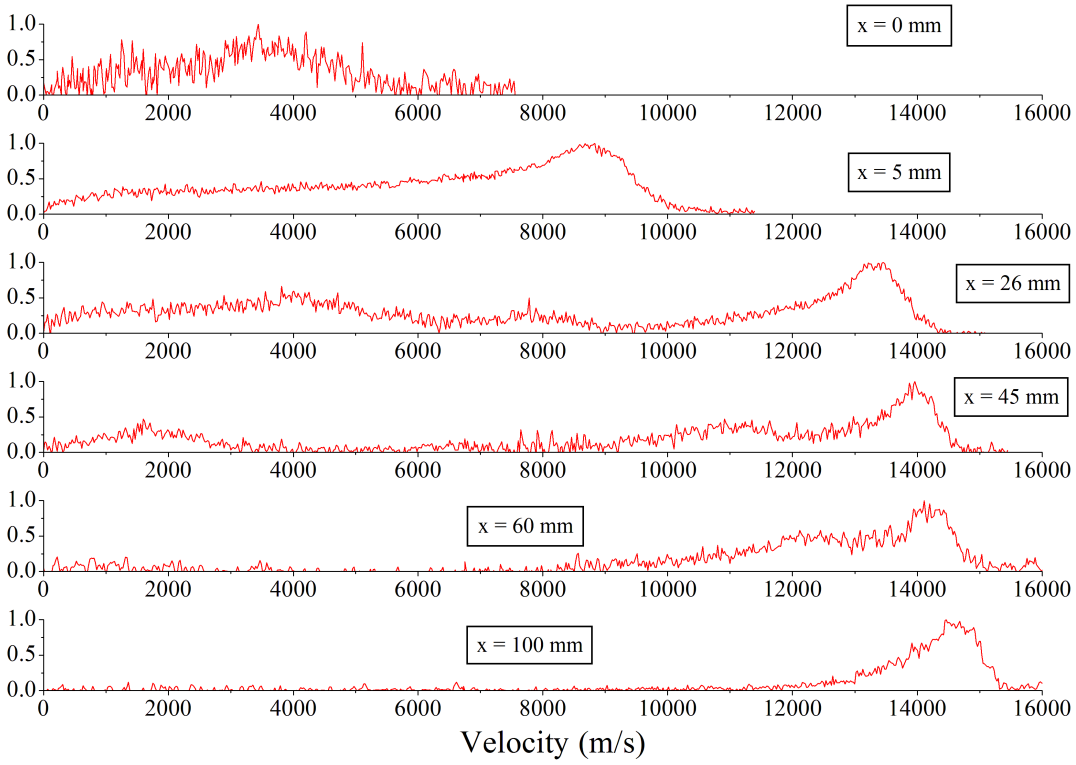

Figure 6. Xe^+ ion VDFs extracted from Fig.5. Each profile in this figure corresponds to a vertical line in the 2D map.

magnitude was the standard one, B_0.

The acceleration of the main fraction of ions is clearly visible from the channel exit plane, which corresponds to x = 0 mm, until the limit at x = 100 mm. As can be seen in Fig.6, the Xe^+ ion VDF is broad in the channel exit plane and within few millimeters downstream, which reveals that ionization and accelerations zones overlap.[8,9] The distribution exhibits a significant low velocity wing. These slow ions with velocity below 1000 m/s originate from local ionization of the gas in the very near-field plume, as well as charge-exchange collisions between ions and neutral. Analysis of all VDFs reveals that this slow velocity wing does exist for all examined geometries and magnetic field strength.

Interesting features appear at low velocity downstream the ionization zone. A large fraction of ions, visible from around 30 mm, accelerate and merge with the main beam. Other small peaks appear and accelerate but does not remain strong enough to be distinguished from background noise. This is of great interest since it has never been cited to the best of our knowledge. The large fraction that merge with the main beam could be related to ions coming from the opposite side of the channel. Their velocity is lower than the main bulk as we only measure the axial projection of ions velocity. The velocity of this second beam increases faster than the main one as both ions velocity increases and the angle of the velocity vector with the axis decreases. From 100 mm downstream the channel exit, only one peak is visible.

A broad peak appears with a very low speed compared to the main bulk of ions. Velocity of these ions seems to increase from thermal speed in the channel exit plane up to to maximum around 4500 m/s at 50 mm. Then it decreases down to thermal speed.

No definite conclusions on the origin of these ions have been drawn yet, but several hypotheses can be mentioned. Charge exchange collisions could generate on each side of the channel bulks of slow ions and fast atoms. Atoms with velocity higher than 1000 m/s were not detected though during the neutral velocity investigation. Ion transit time instability may generate this kind of very slow ions but detailed numerical simulations using fluid and hybrid method are required to support this idea. Existence of second ionization area downstream the channel exit plane may also explain the observed VDFs but is hardly convincing since

neutral density drops quickly outside the channel and may not be sufficient to collide with electrons and produce enough ions so that it could be measured by LIF spectroscopy.

Deceleration of ions requires an existing electric field in the opposite direction. Velocity decreases by 1000 m/s within 10 mm. This field should influence the main ion beam, which does not appear in our measurements. Interaction of the ion beams coming from each side of the channel may produce collisions that does not slow down the ions but changes their trajectory. As we only measure the axial projection of ions velocity, this could also explain why we observe a velocity decrease around 50 mm.

In the following subsections we examine the velocity of Xe^+ ions for several anode mass flow, channel widths and magnetic configuration.

B. Influence of ϕ_a and U_d on the axial velocity of Xe^+ ions

Influence of anode mass flow ϕ_a was studied with two xenon mass flows for a fixed geometry ($3S_0$) and magnetic field strength (B_0). Comparison of on-axis velocity profiles is drawn in Fig.7. Final velocity is not affected by the mass flow and ions velocity reaches 14500 m/s. Acceleration pattern is slightly different which can be seen on the electric field profile. The electric field is the derivative of the accelerating potential. Prior to the differentiation operation, each VDF was smoothed through a fit to a cubic spline. The electric field peaks near the channel exit plane, out of the channel exit plane for the highest mass flow. The shift of the electric field peak may be related to be an enhanced ionization efficiency inside the thruster channel. Exact position must be considered cautiously as it is extremely sensitive to fit options. Electric field cancels around 30 mm which is then the end of the acceleration zone. Velocity in the channel exit plane differs greatly, being 6500 m/s with $\phi_a = 1$ mg/s and 8800 m/s with $\phi_a = 2$ mg/s. As final velocity is unchanged, this means that acceleration efficiency is the same with both anode mass flow, but erosion is likely to be larger with $\phi_a = 2$mg/s as ions exit the channel with greater velocity.

Influence of discharge voltage on maximum velocity measured at x = 100 mm was also studied for several mass flows with a fixed channel width and magnetic field strength. Results are displayed in Fig.8. As previously mentioned, the anode mass flow hardly modifies the final velocity whereas it increases as the square root of the discharge voltage.

C. Influence of the channel width with a fixed magnetic field

The on-axis profile of the Xe+ axial velocity component is displayed in Fig.9 for the three geometrical configurations S_0, $2S_0$, and $3S_0$. The magnetic field is fixed to B_0.

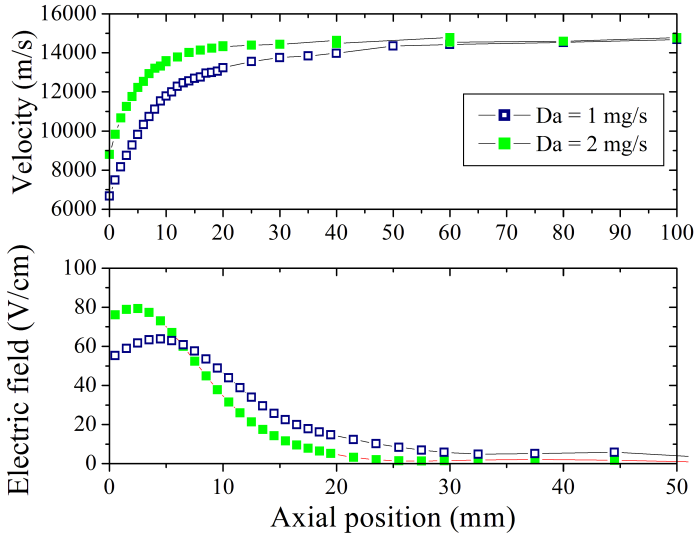

Figure 7. Influence of the anode mass flow on Xe^+ axial velocity (top) and the electric field (bottom). Discharge voltage is 200 V, thruster configuration is (B_0, $3S_0$)

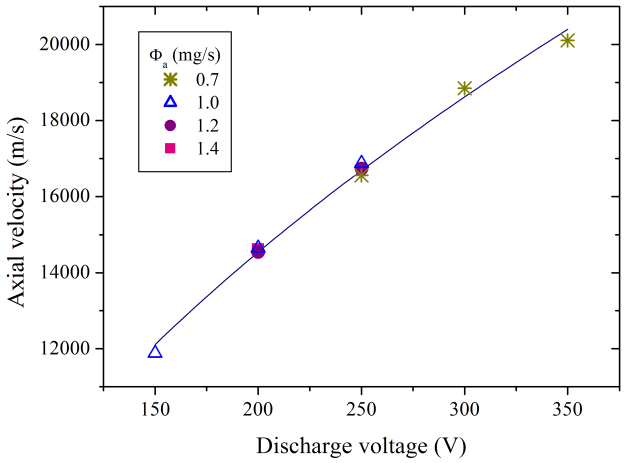

Figure 8. Influence of the discharge voltage and anode mass flow on the velocity at x = 100 mm. Xenon is used as propellant. Thruster configuration is ($3S_0$, B_0).

The anode discharge current is ≈ 0.95 A for each PPI geometry. The three velocity profiles exhibit the same general trend. The Xe^+ ion velocity increases fast over the first 20 mm. Ions still accelerate a little until x = 60 mm. Beyond this distance they travel at constant axial velocity whatever the geometry. A more accurate picture is accessed with the accelerating potential. This potential is obtained from conservation between kinetic energy and potential energy in a collisionless medium[9] . The potential drop experienced by ions inside the channel is given by the kinetic energy in the channel exit plane. This potential is respectively 15 V, 54 V and 41 V for the S_0, $2S_0$ and $3S_0$ configurations. A large part of the acceleration takes place inside the channel where ions are created for the $2S_0$ and $3S_0$ geometries. The overall accelerating potential is computed from the ion final velocity. One finds 146 V for the S_0 geometry, 161 V for the $2S_0$ and 162 V for the $3S_0$ against 200 V applied voltage. The fraction of accelerating potential outside the channel is larger

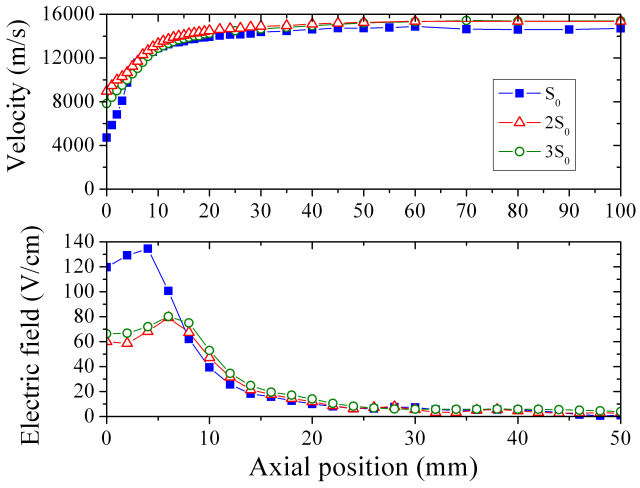

Figure 9. Influence of the channel width on Xe^+ ion velocity (top) and electric field (bottom). Magnetic field magnitude is B_0 and thruster parameters are U_d = 200 V and ϕ_a = 1 mg/s.

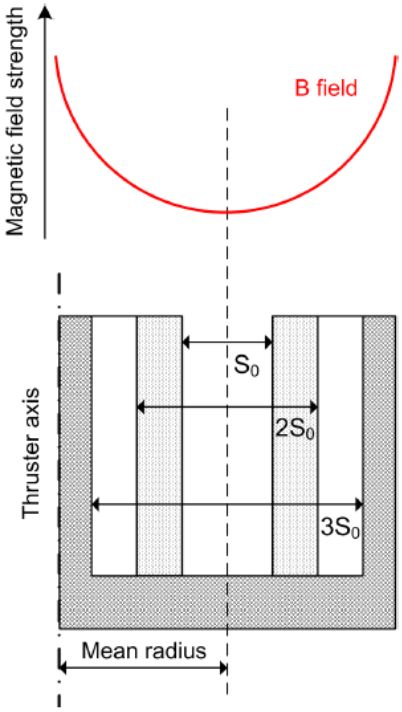

Figure 10. Schematic view of the thruster channel showing the three channel rings. Also shown is a sketch of the magnetic field along the radius

for the S_0 geometry. Nonetheless the two widest channels are more efficient for transforming input energy into kinetic energy. Figure 9 also shows the development of the electric field along the channel axis. The electric field magnitude seems higher for the narrowest channel. For the three geometrical configurations the peak of the electric field distribution is located outside the channel around x = 5 mm. The electric field cancels for the three configurations around x = 50 mm, which is then the end of the acceleration region. Raitses and co-workers obtained similar results with a 2 kW Hall thruster of which the channel width could be changed with ceramic spacers[10] . They examined two geometries: one with a h to d ratio close to the standard one and another one with a larger ratio. The plasma potential profile was measured inside and outside the channel by means of an emissive probe. The potential drop was weaker for the narrow channel, however, the electric field was stronger. They also observed an outward shift of the electric field profile with the narrow channel, which is not noticed in the present study.

Two mechanisms can be put forward to explain the impact of the channel geometry on the ion velocity and the electric field profiles. First, it is a geometrical effect : the surface-to-volume ratio, which is 2/h, corresponds to the ratio of losses to the walls to plasma production. When increasing the channel width h, ion production is favored against wall losses. A preliminary study shows that the propellant utilization increases with h[12,13] . Besides, the ion flux to the walls diminishes. Thus the radial electric field magnitude needed to maintain current equality at walls drops. As a consequence, more energy can be converted into axial electric field and ion acceleration when h augments.

The second mechanism is linked to the magnetized area the plasma is exposed to. As depicted in Fig.10, stretching the channel in radial direction makes the magnetic field intensity larger on the walls. The magnetic field gradient in radial direction is therefore stronger, which enhances the magnetic mirror effect. The latter reduces the electron current to the walls. The magnitude of the electric field within the plasma sheath decreases, which allows a larger potential drop in the axial direction.

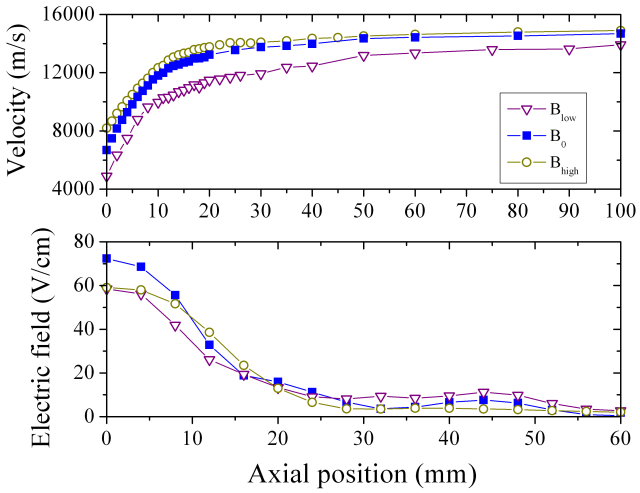

Figure 11. Influence of the magnetic field on Xe^+ ions axial velocity (top) and electric field (bottom). Channel width is $3S_0$, and thruster parameters are U_d = 200 V and ϕ_a = 1 mg/s.

D. Influence of the magnetic field strength for a fixed channel width

The two aforementioned mechanisms are strongly interrelated as by changing the channel width, we modified both geometry and magnetic field magnitude on the walls. In order to clarify their relative contribution, velocity measurements were performed with a fixed geometry for three values of magnetic field. The PPI thruster was fired at 200 V and ϕ_a = 1 mg/s with the $3S_0$ channel configuration for the B_{low}, B_0 and B_{high} magnetic field maps. The discharge current value was, respectively, 1.12 A, 0.97 A and 0.93 A.

The Xe+ ion axial velocity is plotted as a function of the position along the channel axis in Fig.11 for the three B field maps. The shape of the on-axis velocity profile is not much affected by the B field magnitude. On the contrary, the velocity at the channel exhaust as well as the highest ion velocity depend strongly on B magnitude. The two quantities increase when B mounts. The potential drop experienced by ions inside the channel is respectively 16 V, 30 V and 46 V for the B_{low}, B_0 and B_{high} magnetic field strength. The accelerating potential is 132 V, 147 V and 151V in B field ascending order. This measurement series was performed with a new set of $3S_0$ ceramic rings, which could explain the differences that on can note with other data series presented in this study. The gain in accelerating potential when changing B (19 V) is similar to the one obtained when changing h (16 V). The electric field profile along the channel axis is also displayed in Fig.11. The magnetic field strength solely changes the magnitude of the electric field.

When the B-field is increased, the magnetic confinement of electrons inside the channel improves due to an enhanced mirror effect on the walls, therefore plasma-wall interaction reduces. The first fallout is a greater kinetic energy in axial direction as the radial component of the electric field drops. Another result may be a change in electron transport properties throughout the magnetic barrier. As a steep B field radial gradient prevents most of electrons from reaching the wall, the near-wall conductivity is likely to fall down. The electron transverse mobility could then be mostly driven by turbulence.[11] A change in electron transport phenomenon when modifying the channel width or the magnetic field naturally modifies the electric field shape and magnitude.

V. Kr^+ ion velocity profiles

A. Spectroscopic Data

Kr^+ ions metastable 4d $^4F_{7/2}$ state was probed at 820.497 nm (vacuum) and fluorescence light was collected at 462 nm. Fluorescence profile of this transition is shown in Fig.12. It was measured in a low pressure RF discharge. There are five abondant stable isotopes for krypton. Only two of them ^{81}Kr and ^{83}Kr have a

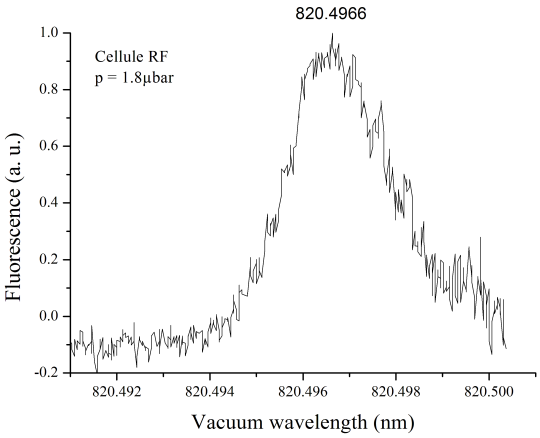

Figure 12. Fluorescence profile of the selected transition of Kr^+ ion in a low pressure RF discharge.

non-zero nuclear spin. Main isotope is ^{84}Kr and hyperfine structure is due to ^{85}Kr.

A complete 2-D map of the evolution with the position of the fluorescence profile has been drawn in Fig.13. The multipeak pattern that was revealed in Fig.5 appears also with krypton even if the decreased signal-to-noise ratio makes it more diffuse and difficult to locate with accuracy. The main acceleration branch makes Kr^+ ions reach a final velocity close to 18 km/s. A second branch appears around 20 mm and merge with the main one at 100 mm downstream the channel exit plane. This feature is similar to the one observed with xenon where the second branch appears at 30 mm from the channel exit plane. This branch could be related to the ion beam coming from the opposite side of the channel as was explained in Section IV A. The fact that the second branch appears from a position closer to the channel exit plane may be a hint that divergence is higher with krypton than with xenon. A diffuse group of ions with velocity close to 5000 m/s seems to decelerate between 50 mm and 70 mm, as was also stated for a location closer to the channel exit plane with xenon. Origin of this group remains unclear. Cathode was fed with krypton and this gas flow could lead to a second ionization zone downstream the channel exit plane.

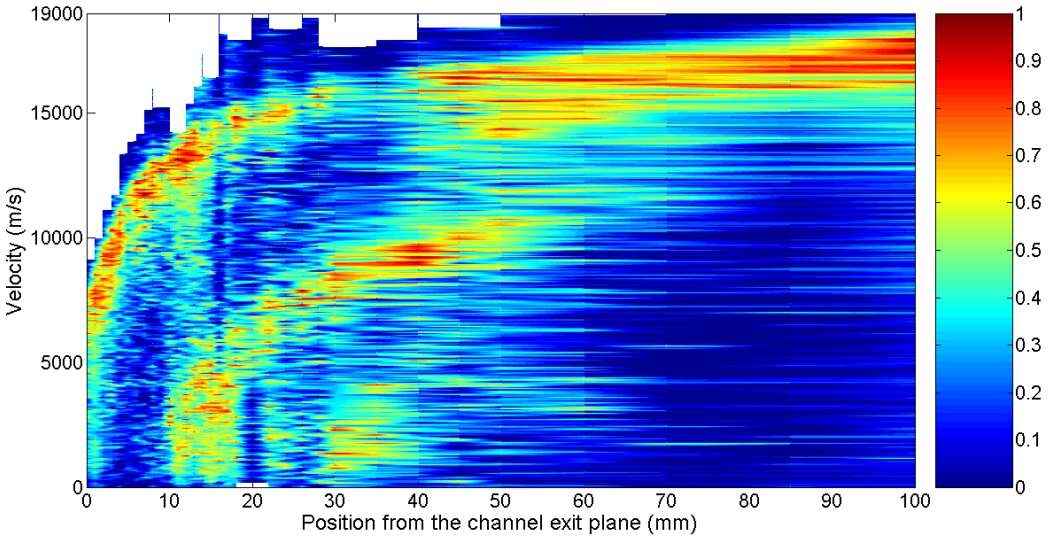

Figure 13. 2D map of the evolution of the Kr^+ ion VDF with the position. Amplitude is given by the colorbar. Thruster running parameters are U_d = 200 V and ϕ_a = 1 mg/s, and configuration is ($3S_0$, B_0)

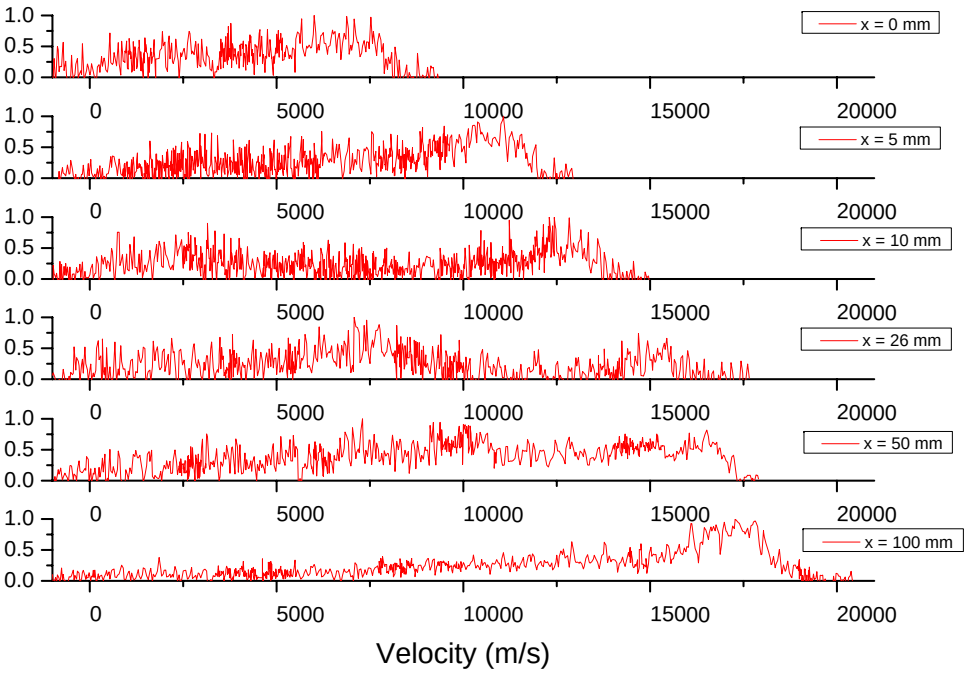

Figure 14. Kr^+ ion fluorescence profiles extracted from Fig.13. Each profile in this figure corresponds to a vertical line in the 2D map.

Several raw fluorescence profiles are also aside in Fig.14 in order to help the understanding of the velocity evolution along the axis of the thruster channel. Discharge voltage was 200 V and discharge current was 1 A with $\phi_a = 1$ mg/s. The largest width ($3S_0$) was used and magnetic field magnitude was the standard one, B_0. The several peaks are clearly visible for each profiles even without smoothing the fluorescence profiles. Time integration constant on the lock-in detection system was raised up to one second instead of 100 ms for xenon.

B. Influence of the channel width with a fixed magnetic field on Kr^+ ion velocity.

Due to its complex isotopic and hyperfine structure, the krypton velocity examined in this section and the following is only the most probable one. Pattern of Kr^+ ion acceleration is very similar to the pattern of Xe^+ ion acceleration. First a zone close to the channel exit plane displays a strong acceleration and the peak of the electric field, followed by a zone where ions experience a free flight regime. Acceleration occurs up to 40 mm which defines the end of the acceleration zone. Final velocity whatever the channel width is close to 18 km/s, higher than xenon ions as krypton mass is 83.8 amu against 136 amu for xenon. Potential conversion efficiency was as high as 81 % with xenon and the $3S_0$ geometry, against 58 % with krypton and the S_0 and $2S_0$, and 56 % with the $3S_0$, which corresponds respectively to 115 V and 111 V of potential with krypton. This is of great interest as the most efficient configuration was the $3S_0$ with xenon which does not seem to be the case with krypton. Electric field profiles are similar with the three geometries even if the peak seems to shift. This is to be considered with great caution as the uncertainty on the measurement of the most probable velocity is greater with krypton than with xenon, which leads to larger uncertainty on the electric field profile and the position of its maximum. More detailed velocity profiles including measurements inside the channel should be able to give more informations on the electric profile change with the geometry.

Influence of the magnetic field was briefly examined with B_0 and B_{high} but profiles were so similar that no conclusion could be drawn out except that increasing the magnetic field magnitude by a factor 1.6 could be not enough to see differences in the acceleration pattern.

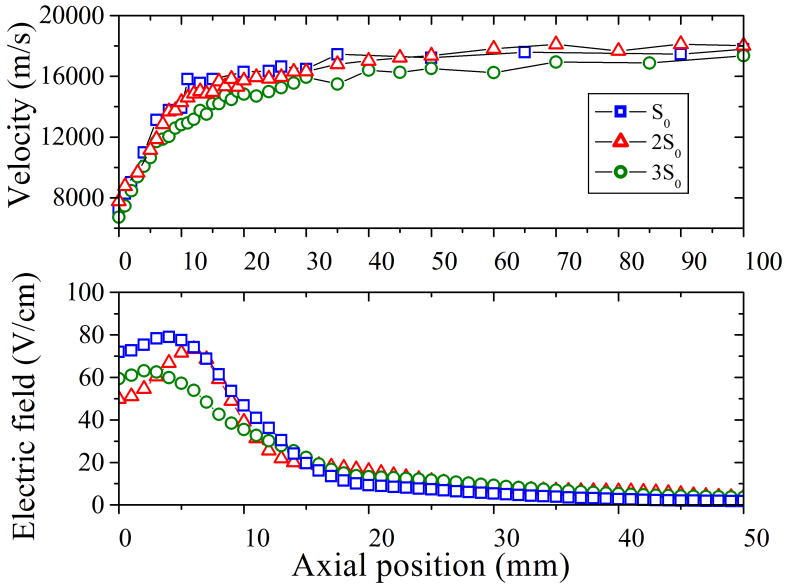

Figure 15. Influence of the channel width on Kr^+ ion velocity (top) and electric field (bottom). Magnetic field magnitude is B_0 and thruster parameters are U_d = 200 V and ϕ_a = 1 mg/s with krypton.

VI. Conclusions

Close examination of Xe^+ VDFs and Kr^+ LIF profiles revealed interesting patterns on beam interactions and the existence of very slow ions downstream the channel exit plane. Systematic study of the complete ion VDFs for Hall thrusters of different sizes could be relevant to study the area where ion beams interact and modify the thruster plume. LIF measurements on xenon atoms gave valuable informations on fast atoms due to selective ionization, charge-exchange collisions inside the channel and slow atoms that may come from the background gas or the cathode. Systematic study of neutrals VDFs could give details on plume interaction with the background noise, cathode gas flow, and on the impact of ground-test facility pressure on the acceleration pattern of ions.

Measurements of the Xe^+ ion axial velocity in the near field plume of a 200 W-class Hall thruster reveal conversion of electrical energy into kinetic energy is enhanced when the channel width is enlarged. The same trend is observed when the magnetic field strength is increased. In the two cases the strong magnetic field nearby the channel walls is responsible for a better electron confinement, hence a reduction in plasma-surface interactions. In addition to a gain in accelerating potential, widening the channel shall therefore improve the thrust efficiency and increase the lifetime. Moreover, as electron and ion bombardment decreases at large h, secondary electron emission could have a little influence on discharge properties. It is therefore of relevance as a follow-up of this work to investigate characteristics of a wide-channel Hall thruster operating at high voltages to improve our understanding of the interaction between secondary electron emission and discharge properties.

Finally, comparison with krypton used as propellant showed that the acceleration pattern is very similar to the pattern of xenon ions velocity. The most efficient geometry seems to be the $2S_0$ which differs greatly from xenon. Systematic study of magnetic field strength have to be carried out to examine more accurately the differences between xenon and krypton used as propellant in the same thruster. Extension of the range of magnetic field strength may be necessary to observe more significant differences.

Acknowledgments

This study was performed in the frame of the CNRS/CNES/SNECMA/Universities joint-research program 3161 entitled 'Propulsion par plasma dans l'espace'. G. Bourgeois benefits from a SNECMA Ph.D. grant. The authors greatly appreciate the skillful technical assistance of L. Peilleron and E. Labrude as well as the fruitful collaboration with N. Sadeghi for investigating Kr^+ ion velocity.

References

[1]Zhurin V.V., Kaufmann H.R., Robinson R.S., "Physics of Closed Drift Thrusters", *Plasma Sources Sci. Technol.* Vol. 8, 1999, pp. R1-R2.

[2]Dannenmayer K. and Mazouffre S., "Elementary Scaling Relations for HAll Effect Thrusters", *J. Propul. Power*, Vol. 27, pp 236-245, 2011.

[3]Guyot M. Renaudin P., Cagan V., and Boniface C., patent FR 07 05658, 2007.

[4]Guyot M. et al., " New concepts for magnetic field generation in Hall effect thrusters",*Proceedings of the 5th International Spacecraft Propulsion Conference*, Heraklion, Crete, 2008.

[5]Pawelec E., Mazouffre S., and Sadeghi N., "Hyperfine stucture of some near-infrared Xe I and Xe II lines ", *Spectrochimica Acta Part B* Vol. 66, 2011, pp. 470-475.

[6]Mazouffre S., Bourgeois G., Garrigues L., and Pawelec E., "A comprehensive study on the atom flow in the cross-field discharge of a Hall thruster", *J. Appl. Phys.*, Vol. 44, 2011, (105203), 8 pp.

[7]Barral S., Makowski K., Peradzynski Z., Gascib N., and Dudeck M. "Wall material effects in stationary plasma thrusters. II. Near-wall and in-wall conductivity", *Phys. Plasmas*, Vol. 10, 2003, pp. 4137-4152.

[8]Mazouffre S., Kulaev V., and Pérez Luna J., "Ion Diagnostics of a discharge in crossed electric and magnetic fields for electric propulsion", *Plasma Sources Sci. Technol.*, Vol. 18, 034022 (2009).

[9]Gawron D., Mazouffre S., Sadeghi N. and Héron A., "Influence of magnetic field and discharge voltage on the acceleration layer features in a Hall effect thruster", *Plasma Sources Sci. Technol.*, Vol. 17, 025001 (2008).

[10]Raitses Y., Staack D., Keidar M., Fisch N.J., "Electron-Wall Interaction in Hall Thrusters", *Phys. Plasmas*, Vol. 12, 2005, pp. 057104-1,057104-9.

[11]Adam J. C., Heron A., and Laval G., "Study of stationary plasma thrusters using two-dimensional fully kinetic simulations", *Phys. Plasmas*, Vol. 11, Number 1, 2004.

[12]Mazouffre S., Dannenmayer K., and Blank C., "Impact of discharge voltage on wall-losses in a Hall thruster", *Phys. Plasmas*, Vol. 18, 2011, pp. 064501-1,0064501-4.

[13]Lejeune A., Dannenmayer K., Bourgeois G., Mazouffre S., Guyot M., and Denise S., "Impact of the channel width on Hall thruster discharge properties and performances", *32nd International Electric Propulsion Conference*, Wiesbaden, Germany, 2011, paper 019.